Biosensors and Bioelectronics 267 (2025) 116790

Contents lists available at ScienceDirect

Biosensors and Bioelectronics

journal homepage: www.elsevier.com/locate/bios

# Enhancing cardiovascular health monitoring: Simultaneous multi-artery cardiac markers recording with flexible and bio-compatible AlN piezoelectric sensors

Marco Cinquino [a,*], Suleyman Mahircan Demir [a,d], Angela Tafadzwa Shumba [a,b], Enrico Junior Schioppa [c], Luca Fachechi [a], Francesco Rizzi [a], Antonio Qualtieri [a], Luigi Patrono [b], Vincenzo Mariano Mastronardi [a,b,1,**], Massimo De Vittorio [a,b,1]

[a] Center for Biomolecular Nanotechnologies, Istituto Italiano di Tecnologia, Arnesano, LE, 73010, Italy
[b] Department of Innovation Engineering, University of Salento, Lecce, LE, 73100, Italy
[c] Inmatica S.p.A., BE-Pilot Palace, Strada Comunale Tufi, Monteroni di Lecce, LE, 73047, Italy
[d] Department of Electronics and Telecommunications, Politecnico di Torino, Corso Duca degli Abruzzi, Torino, TO, 10129, Italy

ARTICLE INFO

*Keywords:*
Flexible piezoelectric sensor
Aluminum nitride
Health monitoring
Cardiovascular parameters
Heart rate
Blood pressure
Pulse wave velocity

ABSTRACT

Continuous monitoring of cardiovascular parameters like pulse wave velocity (PWV), blood pressure wave (BPW), stiffness index (SI), reflection index (RI), mean arterial pressure (MAP), and cardio-ankle vascular index (CAVI) has significant clinical importance for the early diagnosis of cardiovascular diseases (CVDs). Standard approaches, including echocardiography, impedance cardiography, or hemodynamic monitoring, are hindered by expensive and bulky apparatus and accessibility only in specialized facilities. Moreover, noninvasive techniques like sphygmomanometry, electrocardiography, and arterial tonometry often lack accuracy due to external electrical interferences, artifacts produced by unreliable electrode contacts, misreading from placement errors, or failure in detecting transient issues and trends. Here, we report a bio-compatible, flexible, noninvasive, low-cost piezoelectric sensor for continuous and real-time cardiovascular monitoring. The sensor, utilizing a thin aluminum nitride film on a flexible Kapton substrate, is used to extract heart rate, blood pressure waves, pulse wave velocities, and cardio-ankle vascular index from four arterial pulse sites: carotid, brachial, radial, and posterior tibial arteries. This simultaneous recording, for the first time in the same experiment, allows to provide a comprehensive cardiovascular patient's health profile. In a test with a 28-year-old male subject, the sensor yielded the SI = 7.1 ± 0.2 m/s, RI = 54.4 ± 0.5 %, MAP = 86.2 ± 1.5 mmHg, CAVI = 7.8 ± 0.2, and seven PWVs from the combination of the four different arterial positions, in good agreement with the typical values reported in the literature. These findings make the proposed technology a powerful tool to facilitate personalized medical diagnosis in preventing CVDs.

## 1. Introduction

Cardiovascular diseases (CVDs), including hypertension, coronary artery disease, and stroke, are the leading cause of death in the world every year, causing approximately 17 million annual global deaths ("Cardiovascular diseases (CVDs)," n.d.; Nabel, 2003). Prevention and timely therapy are today the most effective ways to decrease mortality (Roth et al., 2015). Nowadays, the typical methods employed to detect the presence of a CVD are coronary computed tomography (CT) (Budoff et al., 1996; Han et al., 2016), magnetic resonance imaging (MRI) (A.C. and Y., 2004), intra-arterial catheters (Yoo et al., 2011), cuff-based sphygmomanometers (Man et al., 2022), auscultation (Boulares et al., 2021), electrocardiography (Bhatia and Dorian, 2018; Siontis et al., 2021), and so on (Altintas et al., 2014; Joung et al., 2023). Nevertheless, these techniques still present difficulties, such as high costs and the need for a fixed posture and well-trained personnel for measurement (Avolio

* Corresponding author. Center for Biomolecular Nanotechnologies, Istituto Italiano di Tecnologia, Arnesano, LE, Italy.
** Corresponding author. Department of Innovation Engineering, University of Salento, Lecce, LE, Italy.
*E-mail addresses:* marco.cinquino@iit.it (M. Cinquino), vincenzomariano.mastronardi@unisalento.it (V.M. Mastronardi).
[1] These authors jointly supervised this work: Vincenzo M. Mastronardi, Massimo De Vittorio.

https://doi.org/10.1016/j.bios.2024.116790
Received 29 July 2024; Received in revised form 10 September 2024; Accepted 16 September 2024
Available online 21 September 2024

et al., 2010; Khan Mamun and Elfouly, 2023; Sharma et al., 2017), the risk of exposure to ionizing radiation (Hamilton-Craig et al., 2012; Kitagawa et al., 2008), or, in the case of arterial catheters, the possible risk of infection (McGhee and Bridges, 2002; Rastegar et al., 2020). For this reason, in the last decades, flexible and wearable sensors for collecting physiological parameters have made important progress driven by the goal of facilitating personalized medical diagnosis and therapies (Chen et al., 2021; Kwon and Dong, 2022; Y. Park et al., 2017; Zhang et al., 2023). Among all the sensors, piezoelectric and triboelectric ones have received significant attention because they don't need an external power supply to operate. Moreover, piezoelectric devices have gained more success because of their higher response to strain (or rather higher piezoelectric charge density at the same strain level) and higher durability than their triboelectric counterparts (Huang et al., 2023). Due to these advantages, piezoelectric sensors have been employed in the noninvasive detection of CVDs by measuring several cardiovascular parameters such as heart rate (A et al., 2022; D. Y. Park et al., 2017; Setyowati et al., 2017), continuous blood pressure (BP) (Dagdeviren et al., 2014; Kim et al., 2023; Li et al., 2023; Min et al., 2023; Tian et al., 2024; Wang et al., 2018; Yi et al., 2022a), heart sounds (Qu et al., 2021; Shumba et al., 2024), and pulse wave velocity (PWV) (Chen et al., 2019; Gatkine et al., 2013; Katsuura et al., 2017; Kim et al., 2023; Wang et al., 2018). Nevertheless, piezo-sensor applications in healthcare remain challenging and have some drawbacks. Interesting outcomes reported in the literature are achieved by exploiting piezoelectric sensors based on lead zirconate titanate ($Pb[Zr_xTi_{1-x}]O_3$, PZT) (Dagdeviren et al., 2014; Li et al., 2023; Min et al., 2023; D. Y. Park et al., 2017; Wang et al., 2018; Yi et al., 2022a) material, which, despite the high piezoelectric coefficient, is highly toxic due to the presence of lead (Pb) (Maeder et al., 2004). Its toxicity is further enhanced due to its evaporation during calcination and sintering in the production phase, causing environmental pollution (Ibn-Mohammed et al., 2017). During fabrication, other proposed sensors (Chen et al., 2019; Tian et al., 2024) employ dangerous and toxic reagents such as hydrofluoric acid (HF) or N,N-dimethylformamide (DMF). Aluminum Nitride (AlN), grown on a flexible Kapton substrate, presents several advantages compared to other piezoelectric materials, such as better compatibility with standard fabrication processes, high electromechanical coupling (Giordano et al., 2009), high resistivity (Eom and Trolier-McKinstry, 2012), no-toxicity due to its lead-free nature, and high thermal stability (Abid et al., 1986). This paper describes a flexible and non-toxic AlN-based piezoelectric sensor that can monitor cardiovascular parameters without risks to patient health and the environment. To achieve a larger view of patient health, the developed sensors are placed on four body locations: (i) carotid, (ii) wrist, (iii) elbow, and (iv) ankle through a skin-safe and fully compatible pressure-sensitive adhesive (Derma-Tac™) film. From the acquired piezo-signals, heart rate, blood pressure waves, mean arterial pressure (MAP), stiffness index (SI), reflection index (RI), seven pulse wave velocities (PWVs), and cardio-ankle vascular index (CAVI) are calculated. Our results match the values reported in the literature and provide a wide view of a subject's state of health. This study furnishes a safer and bio-compatible alternative to measure cardiovascular parameters and can be considered a new step toward the personalized prevention and early diagnosis of CVDs.

## 2. Materials and methods

### 2.1. Sensor fabrication

As reported by Natta et al. (Natta et al., 2021, 2022), the microfabrication process starts with laminating the substrate (Kapton foil) on a silicon (Si) wafer using a thin PDMS sticking layer. The heterostructure was sputtered onto Kapton foil and patterned by optical lithography and chemical dry etching. In particular, the AlN interlayer (120 nm) was deposited using a pure Al target (99.9995%). The AlN interlayer provided a template to reduce the amorphous polyimide surface and promote higher columnar orientation of the grown piezoelectric AlN film. The Mo bottom electrode (200 nm) was deposited in the same run using a pure Mo target (99.95%). The patterning of Mo bottom electrode and AlN interlayer was performed by dry etching with ICP-RIE (Inductively Coupled Plasma - Reactive Ion Etching). The AlN piezoelectric film and top Mo electrode were deposited in the same run. The piezoelectric AlN film was sputtered without heating the substrate, using the same Al target as AlN interlayer. The Mo top layer was sputtered exploiting the same conditions of the bottom electrode. These two films were finally patterned by the ICP-RIE etching system. After the patterning step, the multilayered stack was uniformly coated with a 1 μm-thick Parylene film deposited by chemical vapor coating (Specialty Coating System PDS, 2010 Labcoater). The electrical shielding is manufactured using a lift-off process. A thin titanium layer (Ti, 30 nm) is added using sputtering system, before the deposition of Mo (400 nm) in the same run, to improve the adhesion between the metal and the parylene layer. After the lift-off, another 1 μm-thick Parylene film is deposited by chemical vapor coating (Specialty Coating System PDS, 2010 Labcoater) to provide electrical insulation and waterproofing. Vias to the contact pads for the bottom electrode and the signal electrode were then opened through the Parylene layer by oxygen plasma etching. The device was finally cut and peeled off from the rigid Si substrate. The final device had a thickness of about 30 μm and a total area of 2 $cm^2$.

### 2.2. Sensor packaging and electrical connections

A custom-made electric pad is attached to the sensor through a z-conductive tape purchased from 3M™. AlN sensor charge output is converted into voltage using a Kistler 5165A charge amplifier. The gain of the Kistler is 0.1 V/pC. A 0.5 Hz high pass filter and a 40 Hz low pass filter are employed during the acquisitions. The amplifier outputs are also connected to a Tektronix MDO4104-3 oscilloscope to allow signal visualization. An Olimex Shield-EKG-EMG open-source hardware board records the ECG signal while an OMRON M3 Comfort (HEM-7154-E) is employed to acquire momentary blood pressure and heart rate.

### 2.3. Acquisitions and data analysis

The piezoelectric and ECG signals are carried out on a healthy subject, a male of age 28. Written informed consent is obtained from all human subjects. All measurements are carried out on the same subjects when sitting. Piezoelectric sensors are applied to four subjects' body locations: carotid, wrist, elbow, and ankle. ECG is measured on the chest for all cases. All signals acquired through the piezoelectric sensors are denoised using a third-order IIR bandpass filter with a 0.5–8 Hz cutoff frequency.

### 2.4. Measurements on the subject

Ethical review and approval were waived for this study. Study participants were chosen among the study's authors and informed consent was obtained. Parylene C and dermal glue, materials in contact with the skin, are commercially available for this specific use and/or biocompatible.

## 3. Theory and calculations

Fig. 1a shows a schematic illustration of the piezoelectric sensor. Its structure is based on a thin film heterostructure grown on a Polyimide substrate (Kapton® foil) template with an AlN-interlayer (AlN-IL, 120 nm) on the top. The heterostructure consists of a Molybdenum bottom and top electrodes (Mo, 250 nm) with the piezoelectric layer (highly c-axes oriented AlN, 1 μm thick) in between. The whole fabrication process (reported in Materials and Method, Supporting Information) trades on standard microfabrication techniques, including photolithography and sputtering deposition (Natta et al., 2021, 2022). All layers are

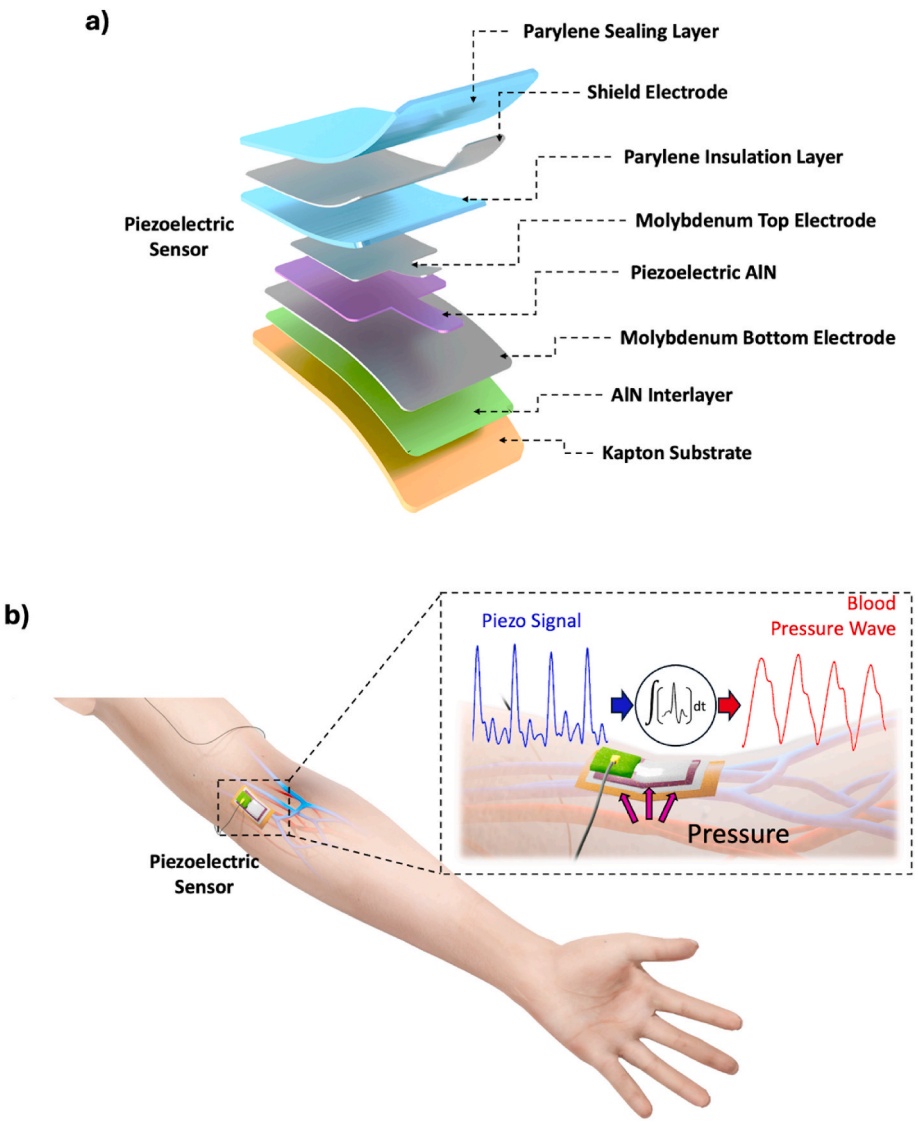


**Fig. 1.** a) Flexible piezoelectric sensor structure; b) schematic illustration of the piezoelectric response generated by the sensor and converted in blood pressure wave.

deposited on Kapton foil (25 μm thick), which was attached to a Si rigid support by a thin layer of PDMS acting as a weak sticking film. The Kapton was chosen as the substrate because of its great resistance to very high deposition temperatures reached during the fabrication process. Kapton is also the reference industry standard in flexible electronics for its reliability, durability, and unique combination of electrical, thermal, chemical, and mechanical properties (Algieri et al., 2018; Guido et al., 2016; Natta et al., 2019). After cutting the sensors with a laser cutter tool and peeling them off from the fabrication substrate, they are applied on the skin through a skin-safe and fully compatible pressure-sensitive adhesive (Derma-Tac™) film. Tests are conducted on the subject under rest conditions. During these tests, the signals acquired by the sensors are generated in response to the heartbeat.

Among all the cardiovascular parameters, blood pressure (BP) is one of the most studied because it can provide information about the stiffness of the vessel wall and vessel diameter, both related to cardiovascular disease (Safar et al., 2015). It is commonly measured through sphygmomanometers, which give only static and time-isolated systolic BP (SBP) and diastolic BP (DBP). On the other hand, continuous BP monitoring due to blood pressure waves (BPWs) allows for a check of how SBP and DBP change in time, providing a more efficient method to track a patient's health. As schematically shown in Fig. 1b, and as reported in the literature (Li et al., 2023; Tian et al., 2024; Yi et al., 2022a), BPWs can be calculated from the piezoelectric signals through the following equation

$$F_{BP}(t) = \frac{1}{\alpha R}\int_0^t V(t)dt + C \quad (1)$$

where $F_{BP}$ is the blood pressure function (in mmHg), $\alpha$ depends on the structure and material properties of the sensor, $R$ is the external electrical resistance, $V$ is the voltage obtained by the conversion of the piezoelectric sensor charge output, and $C$ is a correction factor related to the initial BP of the subject (Tian et al., 2024; Yi et al., 2022a).

Fig. 2a shows the piezoelectric signal acquired from the radial artery of our subject. In Eq. (1), the integral of the voltage provides the shape of the BPW (Fig. 2b-c) while, as already reported (Tian et al., 2024; Yi et al., 2022a), the BP values are obtained calibrating the BPW using the values of SBP and DBP measured through a medical sphygmomanometer. In the first part of each pulse, the pressure increases to the systolic blood pressure due to the blood ejected from the left ventricle to the aorta. The pressure falls to the diastolic blood pressure (DBP) in the second part when the blood flows out from the aorta. The descending part of the waveform is interrupted at the dicrotic notch corresponding

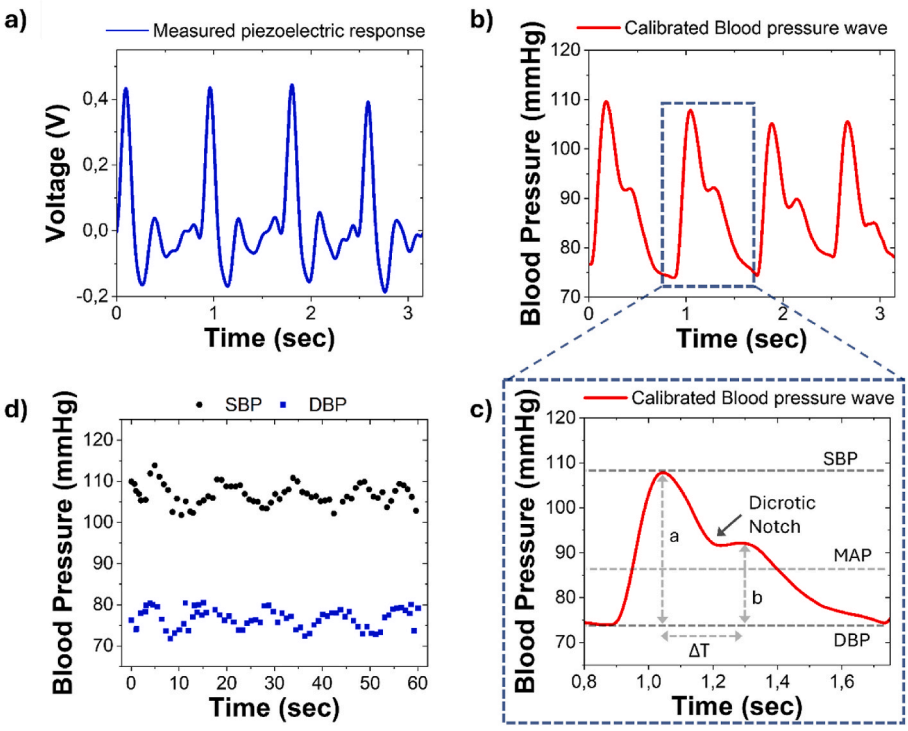


**Fig. 2.** a) Piezoelectric signal collected from the radial artery and b) converted blood pressure waveforms; c) Zoomed waveform extracted from b); d) SBP and DBP trend over 60 s.

to the closure of the aortic valve. Fig. 2b and c show the measured piezoelectric voltage signal acquired from the radial artery and the corresponding BPW estimated with the previously described method after the calibration. In contrast, Fig. 2d shows the trend over time of the SBP and DBP measured through the calibrated BPW.

In addition to BPs, waveforms in Fig. 2b allow us to calculate other important clinical parameters such as the stiffness index (SI), the reflection index (RI), and the mean arterial pressure (MAP), which are defined as follows:

$$SI = \frac{h}{\Delta T} \tag{2}$$

$$RI = \frac{b}{a} \cdot 100\% \tag{3}$$

$$MAP = DBP + \frac{1}{3}(SBP - DBP) \tag{4}$$

where $h$ is the subject's height, $\Delta T$ is the time delay between the systolic and diastolic peaks, while $a$ and $b$ are the magnitudes of the systolic and diastolic peaks, respectively. These derived risk markers are analyzed to evaluate different related cardiovascular risks. In particular, MAP refers to the average arterial BP and is clinically used to detect mild cases of hypertension (Kandil et al., 2023). SI increases with age and is associated with hypertension (Boutouyrie et al., 2021), diabetes-associated arteriosclerosis (Xu et al., 2016), and end-stage renal disease (London, 2018). Finally, RI measures small to medium-sized arterial stiffness and is a predictor of cardiovascular events in a 6,8-year follow-up of well-controlled hypertensive individuals independent of other risk factors (Brillante et al., 2008; Wu and Chen, 2022).

## 4. Results and discussion

In this case, MAP corresponds to 86.2 ± 1.5 mmHg, while SI and RI, estimated on a normalized BPW, are 7.1 ± 0.2 m/s and 54.4 ± 0.5 %, respectively. Proving the healthy state of our 176 cm tall 28-year-old male subject (Brillante et al., 2008; Kandil et al., 2023; Li et al., 2018)). In this study, the piezo-signals and the corresponding extracted BPWs are measured on four arterial pulse sites: carotid, brachial, radial, and posterior tibial arteries (Fig. 3a). All signals are acquired from the same subject and, during all the time required for our tests, no decline in the sensor's performance was observed, proving its long-term durability. Moreover, for every acquisition, the big active area of our sensor (6 mm × 6 mm) allows us to always cover the area of interest, avoiding the error that may occur from misplacement. Fig. S1 presents the scalograms of the piezoelectric signals and fast Fourier transform (FFT) from every analyzed position. The dominant frequencies of 1.11, 1.25, 1.02, and 1.12 Hz, are in good agreement with the typical values, which range between 1 and 1.67 Hz in healthy adults (Yi et al., 2022b). Moreover, they correspond to 66.6, 75, 61.2, and 67 beats per minute (bpm) for carotid, brachial, radial, and posterior tibial arteries, respectively. Since the signals are acquired at different times, the heartbeat recorded at the various positions is slightly different. Fig. 3(f–i) shows how the shape of the BPW changes continuously through the arterial system. In particular, as the sensor is positioned more distally, the dicrotic notch moves further down the BPW. This phenomenon can be explained by considering that when a wave generated from the heart propagates distally, it encounters regions of varying impedance mismatch, causing a reflected wave that goes back towards the heart during late systole and early diastole (Shirwany and Zou, 2010). When this reflected wave travels from an artery farther from the heart, it will take much time to run across the distance, causing a lower dicrotic notch along the BPW.

BPWs can also be employed to calculate the pulse wave velocities (PWVs). PWV is the speed at which the pressure wave travels through the arterial tree and provides information about arterial stiffness (Cavalcante et al., 2011). Among all the cardiovascular parameters, it's one of the most frequently employed to predict cardiovascular diseases in different adult population groups, including those with hypertension (Boutouyrie et al., 2002), renal disease (Guerin et al., 2001), and diabetes (Elias et al., 2017). Several PWVs are reported in the scientific literature, and the reported values mainly depend on the start and

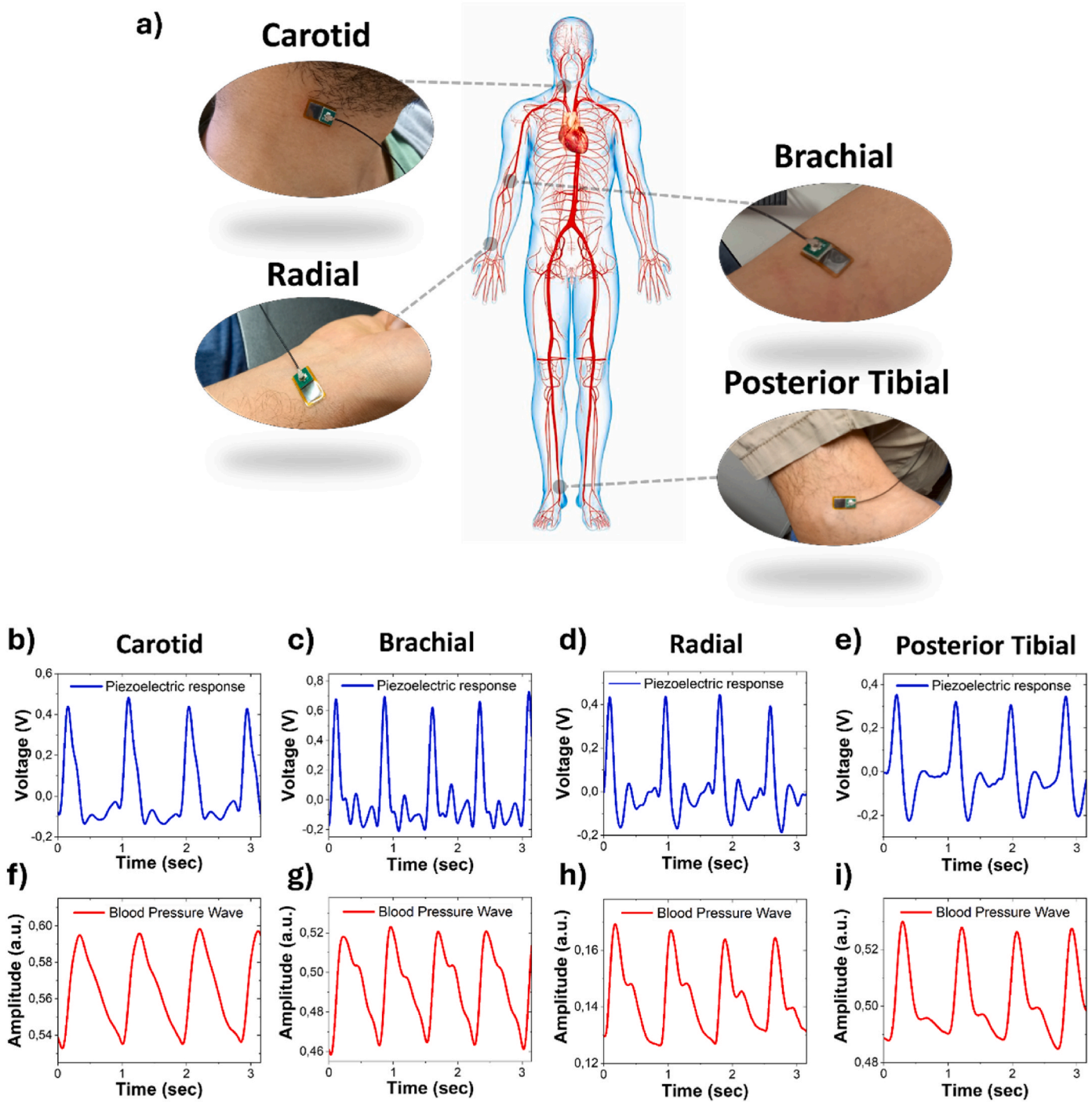


**Fig. 3.** a) Schematic illustration of the measured arterial pulse sites. Piezoelectric signals (b–e) and corresponding blood pressure waves (f–i) are collected from the carotid (b, f), brachial (c, g), radial (d, h), and posterior tibial (e, i) arteries, respectively.

arrival points of the pressure wave (Wang et al., 2023) on the body. In this respect, the PWV can be measured as the difference between the electrocardiogram (ECG) and the piezoelectric signals according to the following equation:

$$PWV = \frac{D}{PAT} \tag{5}$$

where $D$ is the distance between the area of the ECG electrodes and the piezoelectric sensor whereas the pulse arrival time ($PAT$) is the time delay between the R-peak of the acquired ECG and the onset of a pulse in the BPW (Dhillon and Banet, 2019). On the other hand, when the PWV is measured using two piezoelectric sensors placed at two different sites, the equation becomes:

$$PWV = \frac{L}{PTT} \tag{6}$$

where $L$ is the path length between the two sites and the pulse transit time ($PTT$) is the time delay in the pressure wave's arrival at the two positions (Liu et al., 2021). In this study, we used the BPWs shown in Fig. 3 and the synchronized ECG signals (acquired on the chest for all cases) to calculate seven different values of the PWVs. Fig. 4a presents a schematic illustration of the measurements. As seen in Fig. 4b-c, in the

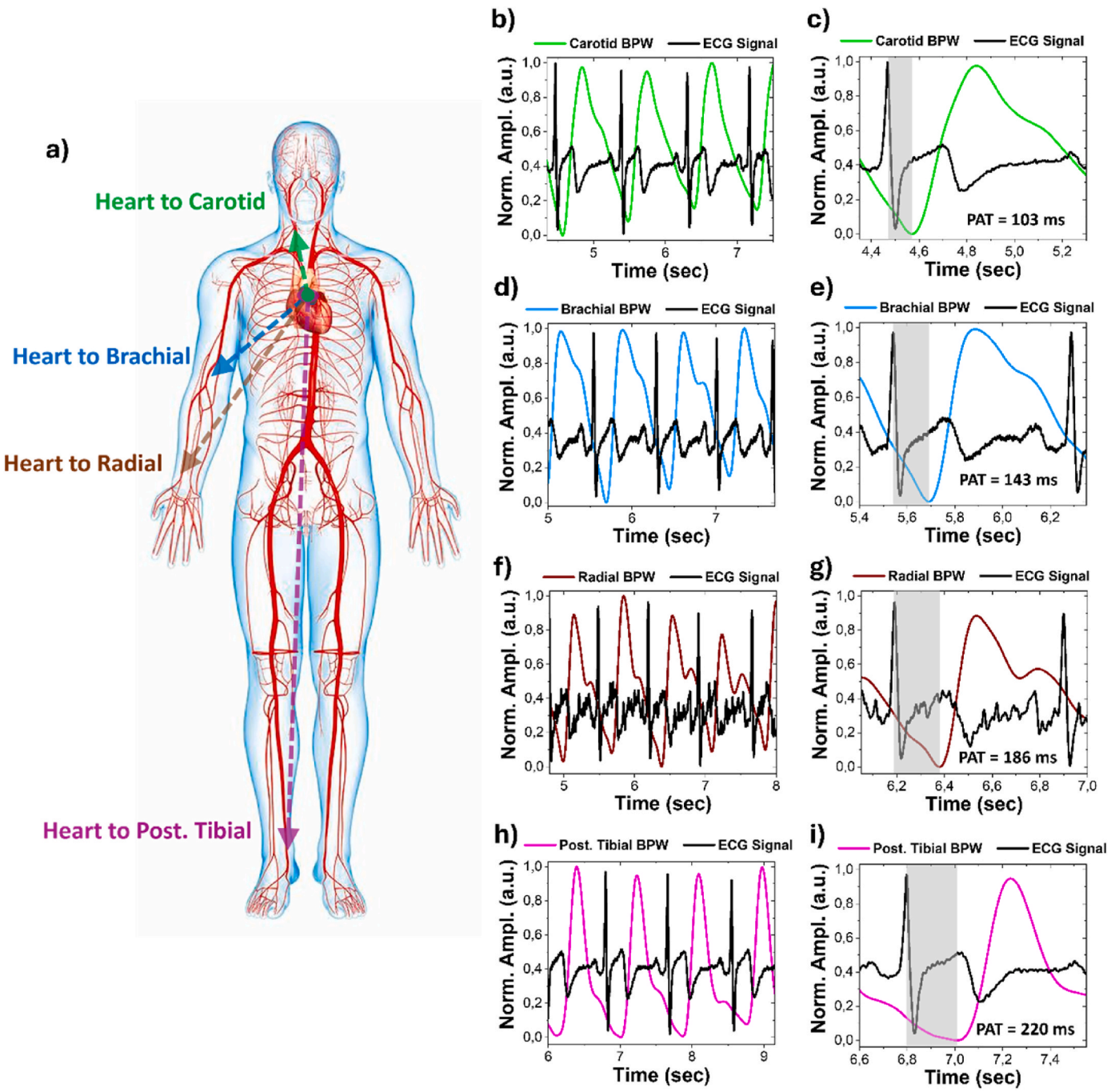


**Fig. 4.** a) Schematic illustration of the measured PWVs using simultaneously an ECG sensor placed on the chest and piezoelectric sensors positioned on b) carotid, d) brachial, f) radial, and h) posterior tibial arteries; c, e, g, i) Zoomed waveform extracted from b), d), f), and h).

case of heart-carotid PWV (*hcPWV,* green line in Fig. 4a), *D* and *PAT* are 22 cm and 103 ± 5 ms, respectively, resulting in a *hcPWV* = 2.1 ± 0.1 m/s. In heart-brachial PWV (*hbPWV*, Fig. 4d-e and blue line in Fig. 4a), *D* and *PAT* increase to 44 cm and 143 ± 5 ms, providing a *hbPWV* = 3.1 ± 0.1 m/s. Moving distally to heart-radial PWV (*hrPWV,* Fig. 4f-g and brown line in Fig. 4a), *D* and *PAT* are 70 cm and 186 ± 5 ms, resulting in a *hrPWV* = 3.8 ± 0.1 m/s. Finally, in heart-tibial PWV (*htPWV*, Fig. 4h-i and magenta line in Fig. 4a), *D* and *PAT* become 155 cm and 220 ± 3 ms while *htPWV* = 7.0 ± 0.1 m/s. In addition, acquiring the piezoelectric signals from the brachial and radial arteries simultaneously (as shown in Fig. S2) it is possible to evaluate the brachial-radial PWV (*brPWV*). As shown in Figs. S3(a–b), brachial and radial BPWs have a *PTT* = 24 ± 3 ms, with *L* = 26 cm, leading to a *brPWV* = 10.8 ± 1.4 m/s. Placing sensors on brachial and posterior tibial arteries at the same time, we are also able to measure the brachial-ankle PWV (baPWV). In this case L = 144 cm and, as shown in Figs. S3(c–d), PTT = 100 ± 5 ms, providing a baPWV = 14.4 ± 0.7 m/s. Lastly, thanks to piezosignals from carotid and radial arteries we measured the carotid-radial PWV (crPWV) which, due to an L = 69 cm and a PTT = 84 ± 6 ms (Figs. S3(e–f)), results to be equal to 8.2 ± 0.6 m/s.

The *htPWV*, also known as heart-ankle PWV (*haPWV*) (Rico Martín et al., 2020), is also used to measure the cardio-ankle vascular index (CAVI). This parameter evaluates the stiffness of the arterial tree from the origin of the aorta to the ankle, and it's considered a predictor marker of CVDs (Matsushita et al., 2019). High CAVI values reflect the presence of several risk factors, such as hypertension (Hayashi et al.,

2015), diabetes mellitus (Ibata et al., 2008), and dyslipidemia (Satoh et al., 2008). Knowing the *htPWV*, the CAVI parameter can be calculated as:

$$CAVI = \frac{2\rho}{\Delta P} \cdot \left( ln \frac{SBP}{DBP} \right) \cdot htPWV^2 \quad (7)$$

where $\rho$ is the blood density, and $\Delta P$ = SBP – DBP. CAVI values, according to age and gender, are classified as normal (CAVI <8), borderline (8 ≤ CAVI <9), and abnormal (CAVI ≥9) (Rico Martín et al., 2020). For the 28-year subject under test, with an SBP and DBP of 116 and 73 mmHg, respectively, the resulting CAVI is 7.8 ± 0.2, matching the values previously reported (Shirai et al., 2019). As shown in Table 1, as well as CAVI, other values of health people's PWVs, MAP, SI, and RI acquired with commercial devices have already been reported (Chen et al., 2019; Li et al., 2015; Scalia et al., 2021; Torrado et al., 2011; Wang et al., 2023) and match our results, proving that our sensor is a valid option to check cardiovascular parameters and monitor subjects' health. Moreover, as shown in Table S1 in Supporting Information, unlike the standard commercial devices, our sensor is wearable and more user friendly, allowing it to be placed on the site of interest without a standardized method and the intervention of an operator. Finally, to prove the reproducibility of our measurements, in Table S2 in Supporting Information we provide the heart-radial pulse arrival times (PATs) and the heart-radial pulse wave velocities (hrPWVs) measured on five different healthy subjects. From the values listed in Table S2, it's clear that all the tested subjects have hrPWVs similar to each other and consistent with those already reported in the literature (Wang et al., 2023), demonstrating the reliability of our results.

## 5. Conclusions

This paper proposes an alternative method to monitor cardiovascular parameters by exploiting an innovative and highly sensitive piezoelectric sensor. The bio-compatible, noninvasive, wearable, and flexible device consisting of a Mo/AlN/Mo sandwich structure is a safer option compared to ones previously reported in the literature, which, employing PZT as piezoelectric material, are toxic and pollutants, representing a danger for human and environment health. We have demonstrated that starting from the acquired piezo signal, it's possible to calculate and evaluate the blood pressure waves and several clinical parameters as predictor markers of critical cardiovascular diseases. In addition, with the integration of a standard ECG device, PWVs and CAVI can be measured, allowing the evaluation of central and peripheral arterial stiffness. The results obtained from the acquisitions performed on healthy subjects are in good agreement with those reported in the scientific literature, showing that they can be easily used in a clinical trial to detect the presence of CVDs (even if they were acquired on healthy subjects). These preliminary results pave the way for the use of piezoelectric technology as a very promising method for measuring physiological markers in a safe, non-invasive, non-obtrusive manner and with a significant reduction in energy consumption and costs, allowing for an important leap towards personalized healthcare.

## CRediT authorship contribution statement

**Marco Cinquino:** Writing – original draft, Visualization, Validation, Methodology, Conceptualization. **Suleyman Mahircan Demir:** Data curation. **Angela Tafadzwa Shumba:** Software, Formal analysis. **Enrico Junior Schioppa:** Resources. **Luca Fachechi:** Validation, Investigation. **Francesco Rizzi:** Validation, Investigation. **Antonio Qualtieri:** Methodology. **Luigi Patrono:** Supervision. **Vincenzo Mariano Mastronardi:** Writing – review & editing, Supervision, Conceptualization. **Massimo De Vittorio:** Writing – review & editing, Supervision, Conceptualization.

**Table 1**
Comparison between the cardiovascular parameters measured through our sensors and the ones acquired with commercial devices.

| Parameter | Values - Our Sensor | Values - Commercial Sensor | Commercial Sensor Model | Reference |
|---|---|---|---|---|
| MAP | 86.2 ± 1.5 mmHg | 89 ± 10 mmHg | Pulse Trace system (Micro Medical, Gillingham, Kent, UK) | Brillante et al. (2008) |
| SI | 7.1 ± 0.2 m/s | 7.3 ± 1.3 m/s | Pulse Trace system (Micro Medical, Gillingham, Kent, UK) | Brillante et al. (2008) |
| RI | 54.4 ± 0.5 % | 69 ± 14 % | Pulse Trace system (Micro Medical, Gillingham, Kent, UK) | Brillante et al. (2008) |
| hcPWV | 2.1 ± 0.1 m/s | 2.4 ± 0.5 m/s | Ultrasound Doppler system (iU22, PhilipsUltrasound, Bothell, WA) | Li et al. (2015) |
| hbPWV | 3.1 ± 0.1 m/s | 3.2 ± 0.3 m/s | BP-203RPE III; Omron Colin, Co., Ltd., Tokyo, Japan | Wang et al. (2023) |
| hrPWV | 3.8 ± 0.1 m/s | 4.2 ± 0.4 m/s | BP-203RPE III; Omron Colin, Co., Ltd., Tokyo, Japan | Wang et al. (2023) |
| htPWV | 7.0 ± 0.1 m/s | 8.4 ± 1.4 m/s | Philips Interventional Hemodynamic System with Patient Monitor IntelliVue X3 | Scalia et al. (2021) |
| brPWV | 10.8 ± 1.4 m/s | 8.2 ± 2.2 m/s | BP-203RPE III; Omron Colin, Co., Ltd., Tokyo, Japan | Wang et al. (2023) |
| baPWV | 14.4 ± 0.7 m/s | 12.5 ± 2.1 m/s | BP-203RPE III; Omron Colin, Co., Ltd., Tokyo, Japan | Wang et al. (2023) |
| crPWV | 8.2 ± 0.6 m/s | 8.1 ± 0.2 m/s | Motorola MPX 2050, Motorola Inc., Corporate 1303 E. Algonquin Road, Schaumburg, Illinois, 60196, USA | Torrado et al. (2011) |
| CAVI | 7.8 ± 0.2 | 7.8 ± 1.2 | VaSera System (Fukuda Denshi, Co. LTD) | Shirai et al. (2019) |

## Declaration of competing interest

The authors declared that they have no conflicts of interest to this work.

## Data availability

The data that has been used is confidential.

## Acknowledgement

This work was carried out within the framework of the project "RAISE - Robotics and AI for Socio-economic Empowerment", ECS00000035 and has been supported by European Union - NextGenerationEU PNRR MUR - M4C2 – I1.5 - Avviso "Ecosistemi dell'Innovazione". However, the views and opinions expressed are those of the authors alone and do not necessarily reflect those of the European Union or the European Commission. Neither the European Union nor the European Commission can be held responsible for them. MS and LA thank MUR for having partially supported this research under the PRIN 2022 project ELFIN 2022SJ8HTC. LF, AQ, and MDV are part of RAISE Innovation Ecosystem.

This research is funded and supervised by the Italian Space Agency (Agenzia Spaziale Italiana, ASI) in the framework of the Research Day "Giornate della Ricerca Spaziale" initiative through the contract ASI N. 2023-7-U.0.

## Appendix A. Supplementary data

Supplementary data to this article can be found online at https://doi.org/10.1016/j.bios.2024.116790.

## References


A, S., A, S., Unnikrishnan, A., Pradeep, A., Rajeev, S.P., D, B.S.S., 2022. Design of piezoelectric heart rate monitoring sensor for wearable applications. In: 2022 6th International Conference on Trends in Electronics and Informatics (ICOEI), pp. 1–6. https://doi.org/10.1109/ICOEI53556.2022.9777147.

Abid, A., Bensalem, R., Sealy, B.J., 1986. The thermal stability of AlN. J. Mater. Sci. 21, 1301–1304. https://doi.org/10.1007/BF00553267.

Algieri, L., Todaro, M.T., Guido, F., Mastronardi, V., Desmaële, D., Qualtieri, A., Giannini, C., Sibillano, T., De Vittorio, M., 2018. Flexible piezoelectric energy-harvesting exploiting biocompatible AlN thin films grown onto Spin-coated polyimide layers. ACS Appl. Energy Mater. 1, 5203–5210. https://doi.org/10.1021/acsaem.8b00820.

Altintas, Z., Fakanya, W.M., Tothill, I.E., 2014. Cardiovascular disease detection using bio-sensing techniques. Talanta 128, 177–186. https://doi.org/10.1016/j.talanta.2014.04.060.

Avolio, A.P., Butlin, M., Walsh, A., 2010. Arterial blood pressure measurement and pulse wave analysis—their role in enhancing cardiovascular assessment. Physiol. Meas. 31, R1. https://doi.org/10.1088/0967-3334/31/1/R01.

Bhatia, R.S., Dorian, P., 2018. Screening for cardiovascular disease risk with electrocardiography. JAMA Intern. Med. 178, 1163–1164. https://doi.org/10.1001/jamainternmed.2018.2773.

Boulares, M., Alotaibi, R., AlMansour, A., Barnawi, A., 2021. Cardiovascular disease recognition based on heartbeat segmentation and selection process. Int. J. Environ. Res. Publ. Health. https://doi.org/10.3390/ijerph182010952.

Boutouyrie, P., Chowienczyk, P., Humphrey, J.D., Mitchell, G.F., 2021. Arterial stiffness and cardiovascular risk in hypertension. Circ. Res. 128, 864–886. https://doi.org/10.1161/CIRCRESAHA.121.318061.

Boutouyrie, P., Tropeano, A.I., Asmar, R., Gautier, I., Benetos, A., Lacolley, P., Laurent, S., 2002. Aortic stiffness is an independent predictor of primary coronary events in hypertensive patients. Hypertension 39, 10–15. https://doi.org/10.1161/hy0102.099031.

Brillante, D.G., O'sullivan, A.J., Howes, L.G., 2008. Arterial Stiffness Indices in Healthy Volunteers Using Non-invasive Digital Photoplethysmography, vol. 17. Blood Press, pp. 116–123. https://doi.org/10.1080/08037050802059225.

Budoff, M.J., Georgiou, D., Brody, A., Agatston, A.S., Kennedy, J., Wolfkiel, C., Stanford, W., Shields, P., Lewis, R.J., Janowitz, W.R., Rich, S., Brundage, B.H., 1996. Ultrafast computed tomography as a diagnostic modality in the detection of coronary artery disease. Circulation 93, 898–904. https://doi.org/10.1161/01.CIR.93.5.898.

Cardiovascular diseases (Cvds). [WWW Document], n.d. URL https://www.who.int/news-room/fact-sheets/detail/cardiovascular-diseases-(cvds).

Cavalcante, J.L., Lima, J.A.C., Redheuil, A., Al-Mallah, M.H., 2011. Aortic stiffness: current understanding and future directions. J. Am. Coll. Cardiol. 57, 1511–1522. https://doi.org/10.1016/j.jacc.2010.12.017.

Chen, J., Liu, H., Wang, W., Nabulsi, N., Zhao, W., Kim, J.Y., Kwon, M.K., Ryou, J.H., 2019. High durable, biocompatible, and flexible piezoelectric pulse sensor using single-crystalline III-N thin film. Adv. Funct. Mater. 29, 1–10. https://doi.org/10.1002/adfm.201903162.

Chen, S., Qi, J., Fan, S., Qiao, Z., Yeo, J.C., Lim, C.T., 2021. Flexible wearable sensors for cardiovascular health monitoring. Adv. Healthcare Mater. 10, 2100116. https://doi.org/10.1002/adhm.202100116.

Dagdeviren, C., Su, Y., Joe, P., Yona, R., Liu, Y., Kim, Y.-S., Huang, YongAn, Damadoran, A.R., Xia, J., Martin, L.W., Huang, Yonggang, Rogers, J.A., 2014. Conformable amplified lead zirconate titanate sensors with enhanced piezoelectric response for cutaneous pressure monitoring. Nat. Commun. 5, 4496. https://doi.org/10.1038/ncomms5496.

Dhillon, M.S., Banet, M.J., 2019. In: Solà, J., Delgado-Gonzalo, R. (Eds.), Pulse Arrival Time Techniques BT - the Handbook of Cuffless Blood Pressure Monitoring: A Practical Guide for Clinicians, Researchers, and Engineers. Springer International Publishing, Cham, pp. 43–59. https://doi.org/10.1007/978-3-030-24701-0_5.

Elias, M.F., Crichton, G.E., Dearborn, P.J., Robbins, M.A., Abhayaratna, W.P., 2017. Associations between type 2 diabetes mellitus and arterial stiffness: a prospective analysis based on the Maine-syracuse study. Pulse 5, 88–98. https://doi.org/10.1159/000479560.

Eom, C.B., Trolier-McKinstry, S., 2012. Thin-film piezoelectric MEMS. MRS Bull. 37, 1007–1017. https://doi.org/10.1557/mrs.2012.273.

Gatkine, P., Gatkine, S., Poojary, S., Chaudhary, S., Noronha, S., 2013. Development of piezo-electric sensor based noninvasive low cost Arterial Pulse Analyzer. In: The 6th 2013 Biomedical Engineering International Conference, pp. 1–4. https://doi.org/10.1109/BMEiCon.2013.6687701.

Giordano, C., Ingrosso, I., Todaro, M.T., Maruccio, G., De Guido, S., Cingolani, R., Passaseo, A., De Vittorio, M., 2009. AlN on polysilicon piezoelectric cantilevers for sensors/actuators. Microelectron. Eng. 86, 1204–1207. https://doi.org/10.1016/j.mee.2008.12.075.

Guerin, A.P., Blacher, J., Pannier, B., Marchais, S.J., Safar, M.E., London, G.M., 2001. Impact of aortic stiffness attenuation on survival of patients in end-stage renal failure. Circulation 103, 987–992. https://doi.org/10.1161/01.CIR.103.7.987.

Guido, F., Qualtieri, A., Algieri, L., Lemma, E.D., De Vittorio, M., Todaro, M.T., 2016. AlN-based flexible piezoelectric skin for energy harvesting from human motion. Microelectron. Eng. 159, 174–178. https://doi.org/10.1016/j.mee.2016.03.041.

Hamilton-Craig, C.R., Friedman, D., Achenbach, S., 2012. Cardiac computed tomography—evidence, limitations and clinical application. Heart Lung Circ. 21, 70–81. https://doi.org/10.1016/j.hlc.2011.08.070.

Han, D., Lee, J.H., Hartaigh, B. o, Min, J.K., 2016. Role of computed tomography screening for detection of coronary artery disease. Clin. Imag. 40, 307–310. https://doi.org/10.1016/j.clinimag.2015.07.002.

Hayashi, K., Yamamoto, T., Takahara, A., Shirai, K., 2015. Clinical assessment of arterial stiffness with cardio-ankle vascular index: theory and applications. J. Hypertens. 33. https://doi.org/10.1097/HJH.0000000000000651.

Huang, S., Gao, Y., Hu, Y., Shen, F., Jin, Z., Cho, Y., 2023. Recent development of piezoelectric biosensors for physiological signal detection and machine learning assisted cardiovascular disease diagnosis. RSC Adv. 13, 29174–29194. https://doi.org/10.1039/D3RA05932D.

Ibata, J., Sasaki, H., Kakimoto, T., Matsuno, S., Nakatani, M., Kobayashi, M., Tatsumi, K., Nakano, Y., Wakasaki, H., Furuta, H., Nishi, M., Nanjo, K., 2008. Cardio-ankle vascular index measures arterial wall stiffness independent of blood pressure. Diabetes Res. Clin. Pract. 80, 265–270. https://doi.org/10.1016/j.diabres.2007.12.016.

Ibn-Mohammed, T., Koh, S.C.L., Reaney, I.M., Sinclair, D.C., Mustapha, K.B., Acquaye, A., Wang, D., 2017. Are lead-free piezoelectrics more environmentally friendly? MRS Commun 7, 1–7. https://doi.org/10.1557/mrc.2017.10.

Joung, J., Jung, C.-W., Lee, H.-C., Chae, M.-J., Kim, H.-S., Park, J., Shin, W.-Y., Kim, C., Lee, M., Choi, C., 2023. Continuous cuffless blood pressure monitoring using photoplethysmography-based PPG2BP-net for high intrasubject blood pressure variations. Sci. Rep. 13, 8605. https://doi.org/10.1038/s41598-023-35492-y.

Kandil, H., Soliman, A., Alghamdi, N.S., Jennings, J.R., El-Baz, A., 2023. Using mean arterial pressure in hypertension diagnosis versus using either systolic or diastolic blood pressure measurements. Biomedicines. https://doi.org/10.3390/biomedicines11030849.

Katsuura, T., Izumi, S., Yoshimoto, M., Kawaguchi, H., Yoshimoto, S., Sekitani, T., 2017. Wearable pulse wave velocity sensor using flexible piezoelectric film array. In: 2017 IEEE Biomedical Circuits and Systems Conference (BioCAS), pp. 1–4. https://doi.org/10.1109/BIOCAS.2017.8325551.

Khan Mamun, M.M., Elfouly, T., 2023. Detection of cardiovascular disease from clinical parameters using a one-dimensional convolutional neural network. Bioengineering. https://doi.org/10.3390/bioengineering10070796.

Kim, Y., Lee, J., Hong, H., Park, S., Ryu, W., 2023. Self-powered wearable micropyramid piezoelectric film sensor for real-time monitoring of blood pressure. Adv. Eng. Mater. 25, 2200873. https://doi.org/10.1002/adem.202200873.

Kitagawa, K., Sakuma, H., Nagata, M., Okuda, S., Hirano, M., Tanimoto, A., Matsusako, M., Lima, J.A.C., Kuribayashi, S., Takeda, K., 2008. Diagnostic accuracy of stress myocardial perfusion MRI and late gadolinium-enhanced MRI for detecting flow-limiting coronary artery disease: a multicenter study. Eur. Radiol. 18, 2808–2816. https://doi.org/10.1007/s00330-008-1097-4.

Kwon, S.H., Dong, L., 2022. Flexible sensors and machine learning for heart monitoring. Nano Energy 102, 107632. https://doi.org/10.1016/j.nanoen.2022.107632.

Li, C., Xiong, H., Pirbhulal, S., Wu, D., Li, Z., Huang, W., Zhang, H., Wu, W., 2015. Heart-carotid pulse wave velocity a useful index of atherosclerosis in Chinese hypertensive patients. Med. (United States) 94, 1–6. https://doi.org/10.1097/MD.0000000000002343.

Li, J., Chen, J., Xu, F., 2018. Sensitive and wearable optical microfiber sensor for human health monitoring. Adv. Mater. Technol. 3, 1800296. https://doi.org/10.1002/admt.201800296.

Li, Jian, Jia, H., Zhou, J., Huang, X., Xu, L., Jia, S., Gao, Z., Yao, K., Li, D., Zhang, B., Liu, Y., Huang, Y., Hu, Y., Zhao, G., Xu, Z., Li, Jiyu, Yiu, C.K., Gao, Y., Wu, M., Jiao, Y., Zhang, Q., Tai, X., Chan, R.H., Zhang, Y., Ma, X., Yu, X., 2023. Thin, soft, wearable system for continuous wireless monitoring of artery blood pressure. Nat. Commun. 14, 5009. https://doi.org/10.1038/s41467-023-40763-3.

Liu, W., Song, D., Yao, Y., Qi, L., Hao, L., Yang, J., Ning, H., Xu, L., 2021. Determination of aortic pulse transit time based on waveform decomposition of radial pressure wave. Sci. Rep. 11, 20154. https://doi.org/10.1038/s41598-021-99723-w.

London, G.M., 2018. Arterial stiffness in chronic kidney disease and end-stage renal disease. Blood Purif. 45, 154–158. https://doi.org/10.1159/000485146.

Maeder, M.D., Damjanovic, D., Setter, N., 2004. Lead free piezoelectric materials. J. Electroceram. 13, 385–392. https://doi.org/10.1007/s10832-004-5130-y.

Man, P.-K., Cheung, K.-L., Sangsiri, N., Shek, W.J., Wong, K.-L., Chin, J.-W., Chan, T.-T., So, R.H., 2022. Blood pressure measurement: from cuff-based to contactless monitoring. Healthcare. https://doi.org/10.3390/healthcare10102113.

Matsushita, K., Ding, N., Kim, E.D., Budoff, M., Chirinos, J.A., Fernhall, B., Hamburg, N. M., Kario, K., Miyoshi, T., Tanaka, H., Townsend, R., 2019. Cardio-ankle vascular index and cardiovascular disease: systematic review and meta-analysis of prospective and cross-sectional studies. J. Clin. Hypertens. 21, 16–24. https://doi.org/10.1111/jch.13425.

McGhee, B.H., Bridges, E.J., 2002. Monitoring arterial blood pressure: what you may not Know. Crit. Care Nurse 22, 60–79. https://doi.org/10.4037/ccn2002.22.2.60.

Min, S., Kim, D.H., Joe, D.J., Kim, B.W., Jung, Y.H., Lee, J.H., Lee, B.-Y., Doh, I., An, J., Youn, Y.-N., Joung, B., Yoo, C.D., Ahn, H.-S., Lee, K.J., 2023. Clinical validation of a wearable piezoelectric blood-pressure sensor for continuous health monitoring. Adv. Mater. 35, 2301627. https://doi.org/10.1002/adma.202301627.

Nabel, E., 2003. Cardiovascular disease. N. Engl. J. Med. 349, 60–72. https://doi.org/10.1056/NEJMra035098.

Natta, L., Guido, F., Algieri, L., Mastronardi, V.M., Rizzi, F., Scarpa, E., Qualtieri, A., Todaro, M.T., Sallustio, V., De Vittorio, M., 2021. Conformable AlN piezoelectric

sensors as a non-invasive Approach for Swallowing Disorder assessment. ACS Sens. 6, 1761–1769. https://doi.org/10.1021/acssensors.0c02339.
Natta, L., Lombardi, P., Mastronardi, V., Guido, F., Qualtieri, A., Di Rienzo, M., Vittorio, M. De, 2022. Flexible Piezoelectric Sensor with Integrated Electromagnetic Shield.
Natta, L., Mastronardi, V.M., Guido, F., Algieri, L., Puce, S., Pisano, F., Rizzi, F., Pulli, R., Qualtieri, A., De Vittorio, M., 2019. Soft and flexible piezoelectric smart patch for vascular graft monitoring based on Aluminum Nitride thin film. Sci. Rep. 9, 8392. https://doi.org/10.1038/s41598-019-44784-1.
Park, D.Y., Joe, D.J., Kim, D.H., Park, Hyewon, Han, J.H., Jeong, C.K., Park, Hyelim, Park, J.G., Joung, B., Lee, K.J., 2017a. Self-powered real-time arterial pulse monitoring using Ultrathin epidermal piezoelectric sensors. Adv. Mater. 29, 1–9. https://doi.org/10.1002/adma.201702308.
Park, Y., Shim, J., Jeong, S., Yi, G.-R., Chae, H., Bae, J.W., Kim, S.O., Pang, C., 2017b. Microtopography-guided conductive patterns of liquid-driven graphene nanoplatelet networks for stretchable and skin-conformal sensor array. Adv. Mater. 29, 1606453. https://doi.org/10.1002/adma.201606453.
Qu, M., Yang, D., Chen, X., Li, D., Zhu, K., Xie, J., 2021. Heart sound monitoring based on a piezoelectric mems acoustic sensor. In: 2021 IEEE 34th International Conference on Micro Electro Mechanical Systems (MEMS), pp. 59–63. https://doi.org/10.1109/MEMS51782.2021.9375350.
Rastegar, S., GholamHosseini, H., Lowe, A., 2020. Non-invasive continuous blood pressure monitoring systems: current and proposed technology issues and challenges. Phys. Eng. Sci. Med. 43, 11–28. https://doi.org/10.1007/s13246-019-00813-x.
Rico Martín, S., Vassilenko, V., de Nicolás Jiménez, J.M., Rey Sánchez, P., Serrano, A., Martínez Alvarez, M., Calderón García, J.F., Sánchez Muñoz-Torrero, J.F., 2020. Cardio-ankle vascular index (CAVI) measured by a new device: protocol for a validation study. BMJ Open 10, e038581. https://doi.org/10.1136/bmjopen-2020-038581.
Roth, G.A., Huffman, M.D., Moran, A.E., Feigin, V., Mensah, G.A., Naghavi, M., Murray, C.J.L., 2015. Global and regional patterns in cardiovascular mortality from 1990 to 2013. Circulation 132, 1667–1678. https://doi.org/10.1161/CIRCULATIONAHA.114.008720.
Safar, M.E., O'Rourke, M.F., Frohlich, E.D., 2015. Blood pressure and arterial wall mechanics in cardiovascular diseases. Blood Pressure and Arterial Wall Mechanics in Cardiovascular Diseases. https://doi.org/10.1007/978-1-4471-5198-2.
Satoh, N., Shimatsu, A., Kato, Y., Araki, R., Koyama, K., Okajima, T., Tanabe, M., Ooishi, M., Kotani, K., Ogawa, Y., Group, for the J.O. and M.S.S. (JOMS), 2008. Evaluation of the cardio-ankle vascular index, a new indicator of arterial stiffness independent of blood pressure, in obesity and metabolic syndrome. Hypertens. Res. 31, 1921–1930. https://doi.org/10.1291/hypres.31.1921.
Scalia, A., Ghafari, C., Carlier, S.G., 2021. A new invasive method to assess pulse wave velocity during cardiac catheterization. Eur. Heart J. 42, 2345. https://doi.org/10.1093/eurheartj/ehab724.2345.
Setyowati, V., Muninggar, J., Shanti, N.A.M.R.S., 2017. Design of heart rate monitor based on piezoelectric sensor using an Arduino. J. Phys. Conf. Ser. 795, 12016. https://doi.org/10.1088/1742-6596/795/1/012016.
Sharma, M., Barbosa, K., Ho, V., Griggs, D., Ghirmai, T., Krishnan, S.K., Hsiai, T.K., Chiao, J.-C., Cao, H., 2017. Cuff-less and continuous blood pressure monitoring: a methodological review. Technologies. https://doi.org/10.3390/technologies5020021.
Shirai, K., Suzuki, K., Tsuda, S., Shimizu, K., Takata, M., Yamamoto, T., Maruyama, M., Takahashi, K., 2019. Comparison of cardio–ankle vascular index (CAVI) and CAVI0 in large healthy and hypertensive populations. J. Atherosclerosis Thromb. 26, 603–615. https://doi.org/10.5551/jat.48314.
Shirwany, N.A., Zou, M., 2010. Arterial stiffness: a brief review. Acta Pharmacol. Sin. 31, 1267–1276. https://doi.org/10.1038/aps.2010.123.
Shumba, A.T., Demir, S.M., Mastronardi, V.M., Rizzi, F., De Marzo, G., Fachechi, L., Ros, P.M., Demarchi, D., Patrono, L., De Vittorio, M., 2024. Monitoring cardiovascular physiology using bio-compatible AlN piezoelectric skin sensors. IEEE Access 12, 16951–16962. https://doi.org/10.1109/ACCESS.2024.3359058.
Siontis, K.C., Noseworthy, P.A., Attia, Z.I., Friedman, P.A., 2021. Artificial intelligence-enhanced electrocardiography in cardiovascular disease management. Nat. Rev. Cardiol. 18, 465–478. https://doi.org/10.1038/s41569-020-00503-2.
Tian, G., Deng, W., Yang, T., Zhang, J., Xu, T., Xiong, D., Lan, B., Wang, S., Sun, Y., Ao, Y., Huang, L., Liu, Y., Li, X., Jin, L., Yang, W., 2024. Hierarchical piezoelectric composites for noninvasive continuous cardiovascular monitoring. Adv. Mater. 2313612, 1–11. https://doi.org/10.1002/adma.202313612.
Torrado, J., Bia, D., Zócalo, Y., Farro, I., Farro, F., Valero, M., Armentano, R.L., 2011. Carotid-radial pulse wave velocity as a discriminator of intrinsic wall alterations during evaluation of endothelial function by flow-mediated dilatation. Proc. Annu. Int. Conf. IEEE Eng. Med. Biol. Soc. EMBS 6458–6461. https://doi.org/10.1109/IEMBS.2011.6091594.
Wang, Chonghe, Li, X., Hu, H., Zhang, Lin, Huang, Z., Lin, M., Zhang, Z., Yin, Z., Huang, B., Gong, H., Bhaskaran, S., Gu, Y., Makihata, M., Guo, Y., Lei, Y., Chen, Y., Wang, Chunfeng, Li, Y., Zhang, T., Chen, Z., Pisano, A.P., Zhang, Liangfang, Zhou, Q., Xu, S., 2018. Monitoring of the central blood pressure waveform via a conformal ultrasonic device. Nat. Biomed. Eng. 2, 687–695. https://doi.org/10.1038/s41551-018-0287-x.
Wang, J., Jing, C., Hu, X., Cui, J., Tang, Q., Tu, L., Zhao, S., Huang, J., Guo, D., Li, Y., Xu, J., 2023. Assessment of aortic to peripheral vascular stiffness and gradient by segmented upper limb PWV in healthy and hypertensive individuals. Sci. Rep. 13, 19859. https://doi.org/10.1038/s41598-023-46932-0.
Wu, H.-T., Chen, J.-J., 2022. Calculation of an improved stiffness index using decomposed radial pulse and digital volume pulse signals. J. Personalized Med. https://doi.org/10.3390/jpm12111768.
Xu, M., Huang, Y., Xie, L., Peng, K., Ding, L., Lin, L., Wang, P., Hao, M., Chen, Y., Sun, Y., Qi, L., Wang, W., Ning, G., Bi, Y., 2016. Diabetes and risk of arterial stiffness: a mendelian randomization analysis. Diabetes 65, 1731–1740. https://doi.org/10.2337/db15-1533.
Yi, Z., Liu, Z., Li, W., Ruan, T., Chen, X., Liu, J., Yang, B., Zhang, W., 2022a. Piezoelectric dynamics of arterial pulse for wearable continuous blood pressure monitoring. Adv. Mater. 34, 1–11. https://doi.org/10.1002/adma.202110291.
Yi, Z., Zhang, W., Yang, B., 2022b. Piezoelectric approaches for wearable continuous blood pressure monitoring: a review. J. Micromech. Microeng. 32, 103003. https://doi.org/10.1088/1361-6439/ac87ba.
Yoo, H., Kim, J.W., Shishkov, M., Namati, E., Morse, T., Shubochkin, R., McCarthy, J.R., Ntziachristos, V., Bouma, B.E., Jaffer, F.A., Tearney, G.J., 2011. Intra-arterial catheter for simultaneous microstructural and molecular imaging in vivo. Nat. Med. 17, 1680–1684. https://doi.org/10.1038/nm.2555.
Zhang, T., Liu, N., Xu, J., Liu, Z., Zhou, Y., Yang, Y., Li, S., Huang, Y., Jiang, S., 2023. Flexible electronics for cardiovascular healthcare monitoring. Innov 4, 100485. https://doi.org/10.1016/j.xinn.2023.100485.